Ultrafast Hot Phonon Dynamics in MgB_2 Driven by Anisotropic Electron-Phonon Coupling

Dino Novko,[1,2,*] Fabio Caruso,[3] Claudia Draxl,[3] and Emmanuele Cappelluti[4,†]
[1]Center of Excellence for Advanced Materials and Sensing Devices, Institute of Physics, Bijenička 46, 10000 Zagreb, Croatia
[2]Donostia International Physics Center (DIPC), Paseo Manuel de Lardizabal 4, 20018 Donostia-San Sebastián, Spain
[3]Institut für Physik and IRIS Adlershof, Humboldt-Universität zu Berlin, Berlin, Germany
[4]Istituto di Struttura della Materia, CNR, Division of Ultrafast Processes in Materials (FLASHit), 34149 Trieste, Italy

(Received 6 April 2019; revised manuscript received 25 October 2019; accepted 28 January 2020; published 21 February 2020)

The zone-center E_{2g} modes play a crucial role in MgB_2, controlling the scattering mechanisms in the normal state as well the superconducting pairing. Here, we demonstrate via first-principles quantum-field theory calculations that, due to the anisotropic electron-phonon interaction, a *hot-phonon* regime where the E_{2g} phonons can achieve significantly larger effective populations than other modes, is triggered in MgB_2 by the interaction with an ultrashort laser pulse. Spectral signatures of this scenario in ultrafast pump-probe Raman spectroscopy are discussed in detail, revealing also a fundamental role of nonadiabatic processes in the optical features of the E_{2g} mode.

DOI: 10.1103/PhysRevLett.124.077001

Although MgB_2 is often regarded as a conventional high-T_c superconductor, as described by the Eliashberg theory for phonon-mediated superconductivity, it displays many peculiar characteristics that make it a unique case. Most remarkable is the anisotropy of the electronic and superconducting properties, where electronic states belonging to the σ bands are strongly coupled to phonons, and thus display large superconducting gaps Δ_σ, whereas electronic states associated with the π bands are only weakly coupled to the lattice, and hence exhibit small superconducting gaps Δ_π [1–10]. Such electronic anisotropy is also accompanied by a striking anisotropy in the *phonon* states. The electron-phonon (*e*-ph) coupling is indeed strongly concentrated in few in-plane E_{2g} phonon modes along the $\bar{\Gamma}-\bar{A}$ path of the Brillouin zone [4,11,12], whereas the remaining *e*-ph coupling is spread over all other lattice modes in the Brillouin zone.

Because of its pivotal role in ruling *e*-ph based many-body effects and in the superconducting pairing, the properties of the long-wavelength E_{2g} mode have been extensively investigated, both theoretically and experimentally [12–30]. On the experimental side, Raman spectroscopy has proven particularly suitable for providing fundamental information on the lattice dynamics and on the many-body *e*-ph processes. Particularly debated is the origin of the large phonon linewidth $\Gamma_{E_{2g}} \approx 25$ meV, and of the temperature dependence of both the phonon frequency and linewidth [12–30]. The complexity of identifying the quantum-mechanical origin of these phenomena arises from the concomitance of the *e*-ph interaction, nonadiabaticity, and lattice anharmonicities, in turn responsible for phonon-phonon scattering and thermal expansion. A possible path for tuning selectively only one of these processes is thus highly desirable, in order to disentangle the different mechanisms in action.

Ultrafast time-resolved optical characterizations of MgB_2 with a pump-probe setup were presented in Refs. [31–33], where two different relaxation times were identified in the normal states. In particular, the observed anomalous blueshift at a short time scale of the in-plane plasmon was qualitatively explained in Ref. [33] by assuming that the E_{2g} mode behaves as a *hot* phonon, i.e., a lattice mode with larger population compared with the thermal distribution of the other lattice degrees of freedom (DOF), in analogy with what was recently observed in graphite and graphene [34–42]. A similar scenario was suggested in Ref. [32]. However, the actual observation of hot-phonon physics in MgB_2 was quite indirect, and further compelling evidence is needed.

In this Letter we present a detailed theoretical investigation of the time-resolved Raman spectroscopy of the E_{2g} mode in a pump-probe setup. Using *ab initio* and quantum-field-theory techniques, we predict that nonequilibrium processes in MgB_2 are dominated by strong hot-phonon physics. Several detailed experimental characterizations are suggested which can provide direct and decisive evidence of the hot-phonon dynamics. It is worth stressing that, unlike graphene where the hot-phonon physics stems from the reduced phase space available for *e*-ph scattering (due to the vanishing Fermi area at the Dirac points) [34–42], the hot-phonon properties in MgB_2 are ruled by the strong anisotropy of the *e*-ph coupling, with the most of the coupling strength being concentrated in few phonon modes at the Brillouin zone center. Such a new theoretical paradigm for inducing hot-phonon physics is not limited to MgB_2 but

it is quite general, and it can be applied to different materials in order to elucidate the time-resolved infrared spectroscopy of the zone-center phonon modes in general. Our work paves the way for a direct experimental check of hot phonons in MgB_2 and in other similar materials characterized by a strongly anisotropic e-ph coupling.

Density-functional theory calculations were performed by using the QUANTUM ESPRESSO package [43]. Norm-conserving pseudopotentials were employed with the Perdew-Burke-Ernzerhof exchange-correlation functional [44]. A $24 \times 24 \times 24$ Monkhorst-Pack grid in momentum space and a plane wave cutoff energy of 60 Ry were used for ground-state calculations. The phonon dispersion was calculated on a $12 \times 12 \times 12$ grid using density-functional perturbation theory (DFPT) [45] and the e-ph coupling was computed by using an in-house modified version of the EPW code [46]. Electron and phonon energies, and e-ph coupling matrix elements were interpolated using maximally localized Wannier functions [47]. The phonon self-energy for the $\mathbf{q} = 0$ E_{2g} mode was computed on a $300 \times 300 \times 300$ electron momentum grid, while the Eliashberg function was obtained on a $40 \times 40 \times 40$ grid of electron and phonon momenta.

The phonon dispersion and the e-ph coupling strengths $\lambda_{\mathbf{q}\nu}$ are depicted in Fig. 1(a), and the corresponding phonon density of states and Eliashberg function $\alpha^2F(\omega)$ in Fig. 1(b). Our computed phonon dispersions are in good agreement with previous results [1–5,22,48,49], while the total e-ph coupling strength $\lambda = 0.6$ is smaller than the earlier *ab initio* values ($\lambda \gtrsim 0.7$) [1,4,49–51], but in rather good agreement with experimental estimates [52,53]. Consistent with earlier works [4,11,12], large values of the e-ph coupling are mainly concentrated in the E_{2g} branch in the Brillouin zone center along the $\bar{\Gamma} - \bar{A}$ line. This is reflected in a dominant peak in the Eliashberg function at the corresponding E_{2g} energies $\omega \approx 60$–70 meV. As shown below, such remarkable anisotropy is responsible for the hot-phonon scenario, where the zone-center E_{2g} phonon modes can acquire, under suitable conditions (i.e., by using pump-probe techniques), a population much larger than other underlying lattice DOF.

In order to capture the anisotropy of the e-ph interaction, we model the total Eliashberg function as the sum of two terms, $\alpha^2F(\omega) = \alpha^2F_{E_{2g}}(\omega) + \alpha^2F_{\mathrm{ph}}(\omega)$, where $\alpha^2F_{E_{2g}}(\omega)$ contains the contribution of the hot E_{2g} modes along and around the $\bar{\Gamma} - \bar{A}$ path in the relevant energy range $\omega \in [60{:}75]$ meV (green shaded areas in Fig. 1), while $\alpha^2F_{\mathrm{ph}}(\omega)$ accounts for the weakly coupled cold modes in the remnant parts of the Brillouin zone. The resulting e-ph coupling strengths for the hot and cold modes are $\lambda_{E_{2g}} = 0.26$ and $\lambda_{\mathrm{ph}} = 0.34$, respectively.

With the fundamental input of the anisotropic e-ph coupling, we investigate the rates of the energy transfer between the electron and lattice DOF in a typical

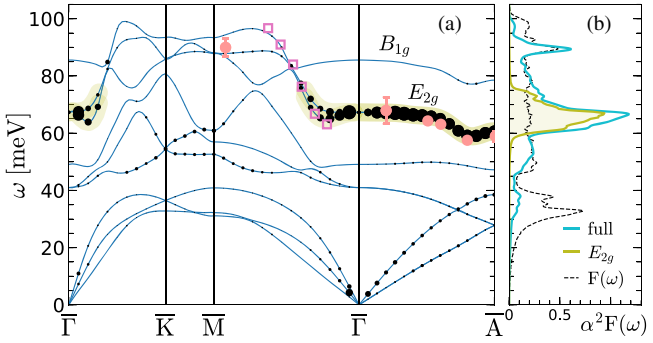

FIG. 1. (a) Plot of the phonon dispersions (solid lines) and e-ph coupling strengths $\lambda_{\mathbf{q}\nu}$, represented by the size of the black circles. Also shown are the experimental phonon energies of the E_{2g} mode close to the $\bar{M}$ point and along the $\bar{\Gamma} - \bar{A}$ path (red circles) [22], as well as along the $\bar{M} - \bar{\Gamma}$ cuts (purple empty squares) [48]. (b) Corresponding phonon density of states $F(\omega)$ (dashed line) and the total Eliashberg function $\alpha^2F(\omega)$ (blue solid line). Green color shows the contribution to the Eliashberg function associated with the hot E_{2g} modes around and along the $\bar{\Gamma} - \bar{A}$ path, $\alpha^2F_{E_{2g}}(\omega)$.

time-resolved pump-probe experiment. As we detail below, energy transfer processes and the hot-phonon physics are driven by the strong anisotropy of the thermodynamical properties of hot and cold modes, i.e., by the remarkable difference in specific heats. This physics thus does not rely on the assumption of effective temperatures for the electronic and lattice DOF. On the other hand, the use of standard three-temperature model appears as a reliable and convenient way to describe these processes in terms of few intuitive quantities [54–58]. The validation of this modeling, compared with the results of a numerical computation using *nonthermal* distributions, is presented in Ref. [59] (for detailed comparison between thermal and nonthermal models see Sec. S2 and Figs. S2 and S3). Characteristic parameters of our description will be thus the effective electronic temperature T_e, the effective temperature $T_{E_{2g}}$ of the hot E_{2g} phonon strongly coupled to the electronic σ bands, and the lattice temperature T_{ph} that describes the effective temperature of the remaining cold phonon modes:

$$C_e \frac{\partial T_e}{\partial t} = S(z,t) + \nabla_z(\kappa \nabla_z T_e) - G_{E_{2g}}(T_e - T_{E_{2g}}) - G_{\mathrm{ph}}(T_e - T_{\mathrm{ph}}), \tag{1}$$

$$C_{E_{2g}} \frac{\partial T_{E_{2g}}}{\partial t} = G_{E_{2g}}(T_e - T_{E_{2g}}) - C_{E_{2g}} \frac{T_{E_{2g}} - T_{\mathrm{ph}}}{\tau_0}, \tag{2}$$

$$C_{\mathrm{ph}} \frac{\partial T_{\mathrm{ph}}}{\partial t} = G_{\mathrm{ph}}(T_e - T_{\mathrm{ph}}) + C_{E_{2g}} \frac{T_{E_{2g}} - T_{\mathrm{ph}}}{\tau_0}. \tag{3}$$

Here C_e, $C_{E_{2g}}$, and C_{ph} are the specific heat capacities for the electron, hot-phonon, and cold-phonon states, respectively.

$G_{E_{2g}}$ (G_{ph}) is the electron-phonon relaxation rate between electronic states and hot (cold) phonon modes, calculated by means of $\alpha^2F_{E_{2g}}$ (α^2F_{ph}). Furthermore κ is the thermal conductivity of electrons and τ_0 is a parameter ruling the anharmonic phonon-phonon scattering between the hot and cold phonon components (for further details see Sec. S1 and Fig. S1 in Ref. [59]). Modeling a typical pump-probe experiment with the photon energy being >1 eV, we assume the pump energy to be transferred uniquely to the electronic DOF by the term $S(z,t) = I(t)e^{-z/\delta}/\delta$, where $I(t)$ is the intensity of the absorbed fraction of the laser pulse (with a Gaussian profile) and δ is the penetration depth. The anisotropic coupling of the e-ph interaction is thus reflected in a different evolution of the three characteristic temperatures. Starting from an initial thermalized system at $T_0 = 300$ K, the energy pumped to the electronic DOF is transferred faster to the E_{2g} phonons than to the other lattice vibrations, leading to an effective temperature $T_{E_{2g}}$ significantly higher than that of the other modes, T_{ph}. Final thermalization between all the lattice DOF occurs on time scales of several picoseconds, as a result of the weak direct phonon-phonon scattering and of the weak coupling between the electronic states and phonon modes other than the E_{2g} ones. In our calculations, the parameters in Eqs. (1)–(3) (with the exception of κ, δ and τ_0) are evaluated numerically from the first-principles calculations [59].

Our calculations predict a very fast increase of $T_{E_{2g}}$ [see Fig. 2(a)], reaching the maximum temperature $T_{E_{2g}}^{\max} \approx 1200$ K with a short delay of 40 fs from the maximum energy transfer to the electronic DOF, consistent with a computed relaxation time $\tau_{E_{2g}} \approx 46$ fs (see Sec. S1 in Ref. [59]). Subsequent thermalization between electrons, hot E_{2g} phonons, and the remaining lattice DOF occurs on a quite longer time scale, ~1 ps [59], where all the DOF thermalize to an average temperature ~400 K [75]. Note that the strong enhancement of $T_{E_{2g}}$ with respect to T_{ph} is not so much due to the difference between $\lambda_{E_{2g}}$ and λ_{ph}, but rather due to the smaller heat capacity $C_{E_{2g}} \ll C_{\mathrm{ph}}$, reflecting the fact that very few E_{2g} modes in $\alpha^2F_{E_{2g}}$ are responsible for a similar coupling as many cold lattice modes in α^2F_{ph}.

The preferential energy transfer to a single phonon mode can be revealed via several experimental techniques. One of the most direct ways is measuring the intensities of the Stokes (S) and anti-Stokes (AS) E_{2g} peaks in Raman spectroscopy, which are related to the Bose-Einstein occupation factor $b(\omega;T) = [\exp(\omega/T) - 1]^{-1}$ via the relations $I_{\mathrm{S}}(T_{E_{2g}}) \propto 1 + b(\omega_{E_{2g}};T_{E_{2g}})$ and $I_{\mathrm{AS}}(T_{E_{2g}}) \propto b(\omega_{E_{2g}};T_{E_{2g}})$, respectively. Assuming to work at zero fluence and room temperature, we predict in Fig. 2(b) an increase of the intensity of the Stokes peak up to a factor 2 [$I_{\mathrm{S}}(T_{E_{2g}})/I_{\mathrm{S}}(300\ \mathrm{K}) \approx 2$], and of the anti-Stokes peak as high as a factor 15 [$I_{\mathrm{AS}}(T_{E_{2g}})/I_{\mathrm{AS}}(300\ \mathrm{K}) \approx 15$]. At the maximum temperature of the hot phonon, the intensity of the anti-Stokes resonance can be as high as 50% of the intensity of the Stokes peak. The experimental investigation of Stokes and anti-Stokes peak intensities in time-resolved Raman spectroscopy may provide also a *direct* way to probe the validity of the hot-phonon scenario by simultaneous measurement of the Stokes and anti-Stokes intensities of the Raman active out-of-plane B_{1g} mode with frequency $\omega_{B_{1g}} \approx 86$ meV. Since this mode is weakly coupled to the electronic states, we expect it to be governed by the cold-phonon temperature T_{ph}, with a drastically different behavior in the time evolution of the Stokes and anti-Stokes peak intensities than the E_{2g} mode (see Sec. S3 and Fig. S4 in Ref. [59]). These spectral signatures constitute a clear fingerprint of hot-phonon physics, suggesting that time-resolved Raman measurements may provide a tool to unambiguously unravel the thermalization mechanisms for systems out of equilibrium.

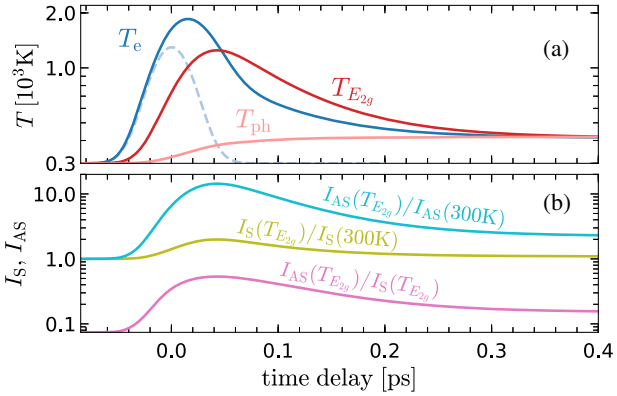

FIG. 2. (a) Time dependence of the electron and phonon effective temperatures T_e, $T_{E_{2g}}$, T_{ph} in MgB_2 as obtained from the three-temperature model. The dashed line shows the pulse profile. The absorbed fluence of the pump pulse is 12 J/m^2, the pulse duration is 45 fs (as in Ref. [33]). (b) Ratios between the intensities of the Stokes (I_{S}) and anti-Stokes (I_{AS}) E_{2g} Raman peaks.

As shown in Refs. [34,42], the peculiar characteristics of hot-phonon dynamics can be traced also through the ω-resolved phonon spectral properties. On the theoretical side, these properties can be properly investigated in the Raman spectra of the E_{2g} mode upon computation of the many-body phonon self-energy $\Pi(\omega;\{T\})$ of the E_{2g} mode at $\mathbf{q} \approx 0$ [76]. Note that, in the real-time dynamics, the phonon self-energy will depend on the *full* set of electron and phonon temperatures $\{T\} = (T_e, T_{E_{2g}}, T_{\mathrm{ph}})$. The full spectral properties can be thus evaluated in terms of the phonon spectral function as [77]

$$B(\omega;\{T\}) = -\frac{1}{\pi}\mathrm{Im}\left[\frac{2\omega_{E_{2g}}}{\omega^2 - \omega_{E_{2g}}^2 - 2\omega_{E_{2g}}\bar{\Pi}(\omega;\{T\})}\right], \quad (4)$$

where $\omega_{E_{2g}} = 67$ meV is the harmonic adiabatic phonon frequency as obtained from DFPT and $\bar{\Pi}(\omega;\{T\})$ is the phonon self-energy for the E_{2g} modes, where, to avoid double counting, the noninteracting adiabatic contribution at $T = 0$ K is subtracted (for more details on the nonadiabatic phonon self-energy see Ref. [59]). The inclusion of many-body effects on the crystal-lattice dynamics via Eq. (4) is reflected by renormalization of the phonon energy $\Omega_{E_{2g}}$ and by the finite phonon linewidth $\Gamma_{E_{2g}}$, which may be computed through solution of the following self-consistent equations: $\Omega^2_{E_{2g}} = \omega^2_{E_{2g}} + 2\omega_{E_{2g}}\bar{\Pi}(\Omega_{E_{2g}};\{T\})$, and $\Gamma_{E_{2g}} = -2\mathrm{Im}\bar{\Pi}(\Omega_{E_{2g}};\{T\})$.

Using such theoretical tools, we evaluate, within the three-temperature model, the time-resolved dynamics of the Raman peak position and of the phonon linewidth, as well as of the full phonon spectral function of the E_{2g} mode in MgB_2 as a function of the pump-probe time delay. A similar approach (however, without time dependence) was used in Ref. [42] for graphene, where the effects of the electronic damping due to the electron-electron interaction were explicitly included in the evaluation of the phonon self-energy. This description is however insufficient in the case of MgB_2 where the electronic damping is crucially governed by the e-ph coupling itself [28,30]. In order to provide a reliable description we evaluate thus the E_{2g} phonon self-energy in a nonadiabatic framework [30] explicitly retaining the e-ph renormalization effects in the Green's functions of the relevant intraband contribution (see Sec. S4 in Ref. [59]). The E_{2g} phonon spectral function is shown in Figs. 3(a) and 3(b) as a function of the time delay, for two different fluences. The corresponding phonon energies $\Omega_{E_{2g}}$ and linewidths $\Gamma_{E_{2g}}$ are summarized in panels (c) and (d). The combined effect of the time evolution of T_e and $T_{E_{2g}}$, T_{ph} results in a nontrivial time dependence of the spectral properties. Our calculations reveal a counterintuitive *reduction* of the phonon linewidth $\Gamma_{E_{2g}}$ right after photoexcitation, followed by a subsequent increase during the overall thermalization with the cold phonon DOF. The time dependence of the phonon frequency shows an even more complex behavior, with an initial redshift, followed by a partial blueshift, and furthermore by a redshift.

In order to rationalize these puzzling results, we analyze in detail the temperature dependence of the phonon spectral properties, decomposing the phonon self-energy into its basic components: interband or intraband terms, and in adiabatic (A) and nonadiabatic (NA) processes. For details see Ref. [59], whereas here we summarize the main results. A crucial role is played by the NA intraband term, which is solely responsible for the phonon damping. Following a robust scheme usually employed for the optical conductivity (see Sec. S4 in Ref. [59]), we can model the effects of the e-ph coupling on the intraband processes in terms of the renormalization function $\lambda(\omega;\{T\})$ and the e-ph particle-hole scattering rate $\gamma(\omega;\{T\})$:

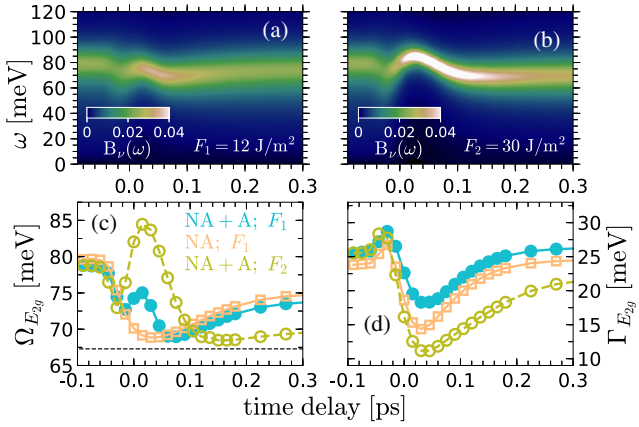

FIG. 3. (a),(b) Intensity of the phonon spectral function $B_{E_{2g}}(\omega;\{T\})$ for $F = 12$ J/m^2 [panel (a)] and for $F = 30$ J/m^2 (panel b). Time evolution of the (c) Raman peak positions and (d) phonon linewidths using the full self-energy for $F = 12$ J/m^2 (full circles) and for $F = 30$ J/m^2 (open circles). Also shown are the results obtained with only the NA intraband term and for $F_2 = 30$ J/m^2 (open squares). The dashed horizontal line in panel (c) shows the adiabatic energy of the E_{2g} mode.

$$\bar{\Pi}^{\mathrm{intra,NA}}(\omega;\{T\}) = \frac{\omega\langle|g_{E_{2g}}|^2\rangle_{T_e}}{\omega[1+\lambda(\omega;\{T\})] + i\gamma(\omega;\{T\})}, \quad (5)$$

where $\langle|g_{E_{2g}}|^2\rangle_{T_e} = -\sum_{n\mathbf{k}\sigma}|g^{nn}_{E_{2g}}(\mathbf{k})|^2\partial f(\varepsilon_{n\mathbf{k}};T_e)/\partial\varepsilon_{n\mathbf{k}}$ [59]. Phonon optical probes at equilibrium are commonly at room (or lower) temperature in the regime $\gamma(\omega;T) \ll \omega[1+\lambda(\omega;T)]$, where the phonon damping $\Gamma_{E_{2g}} \propto \gamma(\Omega_{E_{2g}};T)$. Our calculations predict on the other hand $\gamma(\Omega_{E_{2g}};T_{300\ \mathrm{K}}) \approx 75$ meV, which is close to $\Omega_{E_{2g}}[1+\lambda(\Omega_{E_{2g}};T_{300\ \mathrm{K}})] \approx 85$ meV, resulting in $\Gamma_{E_{2g}} \approx 26$ meV, in good agreement with the experiments [14,15,19] and with the previous calculations [28,30]. The further pump-induced increase of $\gamma(\Omega_{E_{2g}};\{T\}) \gg \Omega_{E_{2g}}[1+\lambda(\Omega_{E_{2g}};\{T\})]$ drives the system into an opposite regime where $\Gamma_{E_{2g}} \propto 1/\gamma(\Omega_{E_{2g}};T)$. In this regime the pump-induced increase of $\gamma(\Omega_{E_{2g}};\{T\})$ results thus in a *reduction* of $\Gamma_{E_{2g}}$, as observed in Fig. 3(d). A similar change of regime is responsible for the crossover from an Elliott-Yafet to the Dyakonov-Perel spin-relaxation, or for the NMR motional narrowing [78,79]. We also note here that the same effects and the change of regime are partially responsible for the overall time dependence of the phonon frequency [see Fig. 3(c)], where the full result (full blue circles) is compared with the one retaining only the nonadiabatic intraband self-energy (open orange squares). The redshift predicted for the latter case is a direct effect of the same change of regime responsible for the reduction of the phonon damping. However, in the real part of the self-energy, adiabatic processes (both intra- and interband) play also a relevant role [59], giving rise to an additional

blueshift (ruled uniquely by T_e) that partially competes with the redshift induced by nonadiabatic intraband processes. Note that actual magnitude of this anomaly depends on the pump fluence [compare full and open circles in Fig. 3(c)]. This dependence can be also used to trace down such adiabatic processes. For a realistic possibility of detecting these spectral features in time-resolved Raman spectroscopy one needs to face the limitations of the time-energy uncertainty [80]. For a time resolution of ~50 fs, comparable with the pulse width, one gets an energy resolution of ~36 meV. While this limitation would prevent the detection of fine structures, the coherent shift of the peak center and the time dependence of the phonon linewidth should be clearly observable [81] (see also Fig. S5 shown in Ref. [59]). Furthermore, the development of alternative techniques based on quantum and statistical correlations [82,83] has shown to provide a promising way to overcome the limitations of the time-energy uncertainty. Therefore, the insights given here along with our *ab initio* method might be of general importance, especially considering that the theoretical framework for deciphering ultrafast phonon dynamics is at the moment not present in the literature.

In conclusion, in this Letter we have presented quantitative and compelling evidence that a hot-phonon scenario dominates the ultrafast carrier dynamics of MgB_2 in time-resolved pump-probe experiments. We further predict the emergence of specific spectral signatures in time-resolved Raman spectroscopy, which may guide the direct experimental verification of a hot-phonon regime in MgB_2. The present analysis is of interest for understanding and controlling the coupling mechanisms in this material, with further relevance for technology. Possible future applications can range from optical probes for sensoring the internal temperature to controlling the heat transfer between electronic and lattice DOF in order to optimizing dissipation processes and interfaces between superconducting and normal metals.

We thank F. Carbone, E. Baldini, L. Benfatto, D. Fausti, A. Perucchi, and P. Postorino for enlightening discussions. D. N. gratefully acknowledges financial support from the European Regional Development Fund for the "Center of Excellence for Advanced Materials and Sensing Devices" (Grant No. KK.01.1.1.01.0001). Financial support by Donostia International Physics Center (DIPC) during various stages of this work is also highly acknowledged. Computational resources were provided by the DIPC computing center.

*dino.novko@gmail.com
†emmanuele.cappelluti@ism.cnr.it

[1] A. Y. Liu, I. I. Mazin, and J. Kortus, Phys. Rev. Lett. **87**, 087005 (2001).
[2] H. J. Choi, D. Roundy, H. Sun, M. L. Cohen, and S. G. Louie, Phys. Rev. B **66**, 020513(R) (2002).
[3] H. J. Choi, D. Roundy, H. Sun, M. L. Cohen, and S. G. Louie, Nature (London) **418**, 758 (2002).
[4] Y. Kong, O. Dolgov, O. Jepsen, and O. Andersen, Phys. Rev. B **64**, 020501(R) (2001).
[5] A. Golubov, J. Kortus, O. Dolgov, O. Jepsen, Y. Kong, O. Andersen, B. Gibson, K. Ahn, and R. Kremer, J. Phys. Condens. Matter **14**, 1353 (2002).
[6] F. Giubileo, D. Roditchev, W. Sacks, R. Lamy, D. Thanh, J. Klein, S. Miraglia, D. Fruchart, J. Marcus, and P. Monod, Phys. Rev. Lett. **87**, 177008 (2001).
[7] S. Tsuda, T. Yokoya, T. Kiss, Y. Takano, K. Togano, H. Kito, H. Ihara, and S. Shin, Phys. Rev. Lett. **87**, 177006 (2001).
[8] X. Chen, M. Konstantinović, J. Irwin, D. Lawrie, and J. P. Franck, Phys. Rev. Lett. **87**, 157002 (2001).
[9] R. Gonnelli, D. Daghero, G. Ummarino, V. Stepanov, J. Jun, S. Kazakov, and J. Karpinski, Phys. Rev. Lett. **89**, 247004 (2002).
[10] D. Mou, R. Jiang, V. Taufour, S. Bud'ko, P. Canfield, and A. Kaminski, Phys. Rev. B **91**, 214519 (2015).
[11] J. M. An and W. E. Pickett, Phys. Rev. Lett. **86**, 4366 (2001).
[12] T. Yildirim, O. Gülseren, J. Lynn, C. Brown, T. Udovic, Q. Huang, N. Rogado, K. Regan, M. Hayward, J. Slusky, T. He, M. Haas, P. Khalifah, K. Inumaru, and R. Cava, Phys. Rev. Lett. **87**, 037001 (2001).
[13] K.-P. Bohnen, R. Heid, and B. Renker, Phys. Rev. Lett. **86**, 5771 (2001).
[14] J. Hlinka, I. Gregora, J. Pokorný, A. Plecenik, P. Kúš, L. Satrapinsky, and Š. Beňačka, Phys. Rev. B **64**, 140503(R) (2001).
[15] A. Goncharov, V. Struzhkin, E.Gregoryanz, J. Hu, R. Hemley, H. k. Mao, G. Lapertot, S. Budko, and P. Canfield, Phys. Rev. B **64**, 100509(R) (2001).
[16] P. Postorino, A. Congeduti, P. Dore, A. Nucara, A. Bianconi, D. D. Castro, S. D. Negri, and A. Saccone, Phys. Rev. B **65**, 020507(R) (2001).
[17] B. Renker, K. Bohnen, R. Heid, D. Ernst, H. Schober, M. Koza, P. Adelmann, P. Schweiss, and T. Wolf, Phys. Rev. Lett. **88**, 067001 (2002).
[18] J. W. Quilty, S. Lee, A. Yamamoto, and S. Tajima, Phys. Rev. Lett. **88**, 087001 (2002).
[19] H. Martinho, C. Rettori, P. Pagliuso, A. Martin, N. Moreno, and J. Sarrao, Solid State Commun. **125**, 499 (2003).
[20] L. Shi, H. Zhang, L. Chen, and Y. Feng, J. Phys. Condens. Matter **16**, 6541 (2004).
[21] D. D. Castro, E. Cappelluti, M. Lavagnini, A. Sacchetti, A. Palenzona, M. Putti, and P. Postorino, Phys. Rev. B **74**, 100505(R) (2006).
[22] A. Shukla, M. Calandra, M. d'Astuto, M. Lazzeri, F. Mauri, C. Bellin, M. Krisch, J. Karpinski, S. M. Kazakov, J. Jun, D. Daghero, and K. Parlinski, Phys. Rev. Lett. **90**, 095506 (2003).
[23] L. Boeri, G. Bachelet, E. Cappelluti, and L. Pietronero, Phys. Rev. B **65**, 214501 (2002).
[24] G. Profeta, A. Continenza, and S. Massidda, Phys. Rev. B **68**, 144508 (2003).
[25] M. Lazzeri, M. Calandra, and F. Mauri, Phys. Rev. B **68**, 220509(R) (2003).

[26] M. Calandra and F. Mauri, Phys. Rev. B **71**, 064501 (2005).
[27] L. Boeri, E. Cappelluti, and L. Pietronero, Phys. Rev. B **71**, 012501 (2005).
[28] E. Cappelluti, Phys. Rev. B **73**, 140505(R) (2006).
[29] L. Simonelli, V. Palmisano, M. Fratini, M. Filippi, P. Parisiades, D. Lampakis, E. Liarokapis, and A. Bianconi, Phys. Rev. B **80**, 014520 (2009).
[30] D. Novko, Phys. Rev. B **98**, 041112(R) (2018).
[31] Y. Xu, M. Khafizov, L. Satrapinsky, P. Kúš, A. Plecenik, and R. Sobolewski, Phys. Rev. Lett. **91**, 197004 (2003).
[32] J. Demsar, R. Averitt, A. Taylor, V. Kabanov, W. Kang, H. Kim, E. Choi, and S. Lee, Phys. Rev. Lett. **91**, 267002 (2003).
[33] E. Baldini, A. Mann, L. Benfatto, E. Cappelluti, A. Acocella, V. Silkin, S. Eremeev, A. Kuzmenko, S. Borroni, T. Tan, X. Xi, F. Zerbetto, R. Merlin, and F. Carbone, Phys. Rev. Lett. **119**, 097002 (2017).
[34] H. Yan, D. Song, K. F. Mak, I. Chatzakis, J. Maultzsch, and T. F. Heinz, Phys. Rev. B **80**, 121403(R) (2009).
[35] S. Berciaud, M. Y. Han, K. F. Mak, L. E. Brus, P. Kim, and T. F. Heinz, Phys. Rev. Lett. **104**, 227401 (2010).
[36] D.-H. Chae, B. Krauss, K. von Klitzing, and J. H. Smet, Nano Lett. **10**, 466 (2010).
[37] S. Butscher, F. Mildea, M. Hirtschulz, E. Malić, and A. Knorr, Appl. Phys. Lett. **91**, 203103 (2007).
[38] H. Wang, J. Strait, P. George, S. Shivaraman, V. Shields, M. Chandrashekhar, J. Hwang, F. Rana, M. Spencer, C. Ruiz-Vargas, and J. Park, Appl. Phys. Lett. **96**, 081917 (2010).
[39] M. Scheuch, T. Kampfrath, M. Wolf, K. von Volkmann, C. Frischkorn, and L. Perfetti, Appl. Phys. Lett. **99**, 211908 (2011).
[40] L. Huang, B. Gao, G. Hartland, M. Kelly, and H. Xing, Surf. Sci. **605**, 1657 (2011).
[41] S. Wu, W.-T. Liu, X. Liang, P. J. Schuck, F. Wang, Y. R. Shen, and M. Salmeron, Nano Lett. **12**, 5495 (2012).
[42] C. Ferrante, A. Virga, L. Benfatto, M. Martinati, D. De Fazio, U. Sassi, C. Fasolato, A. K. Ott, P. Postorino, D. Yoon, G. Cerullo, F. Mauri, A. C. Ferrari, and T. Scopigno, Nat. Commun. **9**, 308 (2018).
[43] P. Giannozzi, S. Baroni, N. Bonini, M. Calandra, R. Car, C. Cavazzoni, D. Ceresoli, G. L. Chiarotti, M. Cococcioni, I. Dabo *et al.*, J. Phys. Condens. Matter **21**, 395502 (2009).
[44] J. P. Perdew, K. Burke, and M. Ernzerhof, Phys. Rev. Lett. **77**, 3865 (1996).
[45] S. Baroni, S. de Gironcoli, A. Dal Corso, and P. Giannozzi, Rev. Mod. Phys. **73**, 515 (2001).
[46] S. Poncé, E. Margine, C. Verdi, and F. Giustino, Comput. Phys. Commun. **209**, 116 (2016).
[47] N. Marzari, A. A. Mostofi, J. R. Yates, I. Souza, and D. Vanderbilt, Rev. Mod. Phys. **84**, 1419 (2012).
[48] A. Q. R. Baron, H. Uchiyama, Y. Tanaka, S. Tsutsui, D. Ishikawa, S. Lee, R. Heid, K.-P. Bohnen, S. Tajima, and T. Ishikawa, Phys. Rev. Lett. **92**, 197004 (2004).
[49] A. Eiguren and C. Ambrosch-Draxl, Phys. Rev. B **78**, 045124 (2008).
[50] M. Calandra, G. Profeta, and F. Mauri, Phys. Rev. B **82**, 165111 (2010).
[51] E. R. Margine and F. Giustino, Phys. Rev. B **87**, 024505 (2013).
[52] F. Bouquet, R. A. Fisher, N. E. Phillips, D. G. Hinks, and J. D. Jorgensen, Phys. Rev. Lett. **87**, 047001 (2001).
[53] Y. Wang, T. Plackowski, and A. Junod, Physica (Amsterdam) **355C**, 179 (2001).
[54] P. B. Allen, Phys. Rev. Lett. **59**, 1460 (1987).
[55] L. Perfetti, P. A. Loukakos, M. Lisowski, U. Bovensiepen, H. Eisaki, and M. Wolf, Phys. Rev. Lett. **99**, 197001 (2007).
[56] C. Lui, K. Mak, J. Shan, and T. Heinz, Phys. Rev. Lett. **105**, 127404 (2010).
[57] S. Dal Conte, C. Giannetti, G. Coslovich, F. Cilento, D. Bossini, T. Abebaw, F. Banfi, G. Ferrini, H. Eisaki, M. Greven, A. Damascelli, D. van der Marel, and F. Parmigiani, Science **335**, 1600 (2012).
[58] J. C. Johannsen, S. Ulstrup, F. Cilento, A. Crepaldi, M. Zacchigna, C. Cacho, I. C. E. Turcu, E. Springate, F. Fromm, C. Raidel, T. Seyller, F. Parmigiani, M. Grioni, and P. Hofmann, Phys. Rev. Lett. **111**, 027403 (2013).
[59] See Supplemental Material at http://link.aps.org/supplemental/10.1103/PhysRevLett.124.077001, which additionally includes Refs. [60–74], for more details on the temperature dependence of the thermodynamical quantities and of the relaxation times for hot and cold lattice modes; on the validation of the effective temperature model; on the analysis of Stokes and anti-Stokes intensities and the E_{2g} phonon self-energy calculations; and on the energy-time resolution discussion.
[60] Z. Lin, L. V. Zhigilei, and V. Celli, Phys. Rev. B **77**, 075133 (2008).
[61] A. Balassis, E. V. Chulkov, P. M. Echenique, and V. M. Silkin, Phys. Rev. B **78**, 224502 (2008).
[62] E. Bauer, C. Paul, S. Berger, S. Majumdar, H. Michor, M. Giovannini, A. Saccone, and A. Bianconi, J. Phys. Condens. Matter **13**, L487 (2001).
[63] S. Brorson, A. Kazeroonian, S. Moodera, D. Face, T. Cheng, E. Ippen, M. Dresselhaus, and G. Dresselhaus, Phys. Rev. Lett. **64**, 2172 (1990).
[64] W. Fann, R. Storz, H. Tom, and J. Bokor, Phys. Rev. B **46**, 13592 (1992).
[65] J. Hohlfeld, S.-S. Wellershoff, J. Güdde, U. Conrad, V. Jähnke, and E. Matthias, Chem. Phys. **251**, 237 (2000).
[66] A. M. Saitta, M. Lazzeri, M. Calandra, and F. Mauri, Phys. Rev. Lett. **100**, 226401 (2008).
[67] F. Caruso, M. Hoesch, P. Achatz, J. Serrano, M. Krisch, E. Bustarret, and F. Giustino, Phys. Rev. Lett. **119**, 017001 (2017).
[68] V. Guritanu, A. Kuzmenko, D. van der Marel, S. Kazakov, N. Zhigadlo, and J. Karpinski, Phys. Rev. B **73**, 104509 (2006).
[69] D. Di Castro, M. Ortolani, E. Cappelluti, U. Schade, N. Zhigadlo, and J. Karpinski, Phys. Rev. B **73**, 174509 (2006).
[70] P. B. Allen, Phys. Rev. B **3**, 305 (1971).
[71] P. B. Allen and R. Silberglitt, Phys. Rev. B **9**, 4733 (1974).
[72] S. Shulga, O. Dolgov, and E. Maksimov, Physica (Amsterdam) **178C**, 266 (1991).
[73] M. Norman and A. Chubukov, Phys. Rev. B **73**, 140501(R) (2006).
[74] D. Novko, Nano Lett. **17**, 6991 (2017).
[75] Note that the time evolution of T_e resembles remarkably the two-τ behavior discussed in Ref. [32], where, however, the

idea of a fast electron-electron thermalization was rejected. The outstanding rise of $T_{E_{2g}}$ is not expected to depend substantially on the effective electron-electron thermalization (see Ref. [59]).

[76] M. Lazzeri and F. Mauri, Phys. Rev. Lett. **97**, 266407 (2006).

[77] F. Giustino, Rev. Mod. Phys. **89**, 015003 (2017).

[78] P. Boross, B. Dóra, A. Kiss, and F. Simon, Sci. Rep. **3**, 3233 (2013).

[79] L. Szolnoki, A. Kiss, B. Dóra, and F. Simon, Sci. Rep. **7**, 9949 (2017).

[80] R. Versteeg, J. Zhu, P. Padmanabhan, C. Boguschewski, R. German, M. Goedecke, P. Becker, and P. M. van Loosdrecht, Struct. Dyn. **5**, 044301 (2018).

[81] D. Fausti, O. Misochko, and P. van Loosdrecht, Phys. Rev. B **80**, 161207(R) (2009).

[82] F. Randi, D. Fausti, and M. Eckstein, Phys. Rev. B **95**, 115132 (2017).

[83] J. Tollerud, G. Sparapassi, A. Montanaro, S. Asban, F. Glerean, F. Giusti, A. Marciniak, G. Kourousias, F. Billè, F. Cilento, S. Mukamel, and D. Fausti, Proc. Natl. Acad. Sci. U.S.A. **116**, 5383 (2019).